Materials and Design 63 (2014) 185–193

Contents lists available at ScienceDirect

Materials and Design

journal homepage: www.elsevier.com/locate/matdes

Effects of scan line spacing on pore characteristics and mechanical properties of porous Ti6Al4V implants fabricated by selective laser melting

Sheng Zhang, Qingsong Wei *, Lingyu Cheng, Suo Li, Yusheng Shi

State Key Lab of Materials Processing and Die & Mould Technology, Huazhong University of Science and Technology, 1037 # Luoyu Road, Wuhan, China

ARTICLE INFO

Article history:
Received 17 February 2014
Accepted 14 May 2014
Available online 24 May 2014

Keywords:
Ti6Al4V
Selective laser melting
Scan line spacing
Mechanical property
Pore
Implant

ABSTRACT

The use of porous structures is gaining popularity in biomedical implant manufacture fields due to its ability to promote increased osseointegration and cell proliferation. Selective laser melting (SLM) is a metal additive manufacturing (MAM) technique capable of producing the porous structure. Adjusting the parameter of scan line spacing is a simple and fast way to gain porous structures in SLM process. By using the medical alloy of Ti6Al4V, we systematically study the influence of the scan line spacing on pore characteristics and mechanical properties of porous implant for the first time. The scanning electron microscope (SEM) results show that the porous Ti6Al4V implants with interconnected pore sizes which ranges from 250 to 450 μm is appropriate for compact bone. The compression strength and modulus of the porous Ti6Al4V implants decrease with the increase of the scan line spacing, and two equations by fitting the data have been established to predict their compression properties. The compressive deformation of the porous Ti6Al4V implants presented an adiabatic shear band (ASB) fracture, which is similar to dense Ti6Al4V owing to the dense thin wall structures. The ability to create both high porosity and strong mechanical properties implants opens a new avenue for fabricating porous implants which is used for load-bearing bone defect repair and regeneration.

1. Introduction

Metal additive manufacturing (MAM) techniques offer an almost unlimited flexibility of geometry and complexity, providing special opportunities for orthopedic and bone implants [1]. Compared to other MAM technologies, selective laser melting (SLM) has the advantage to fabricate metal parts that have mechanical properties comparable to those of bulk materials [2] It allows the manufacturing of complex three-dimensional (3-D) parts by selectively melting successive layers of metal powders on top of each other, using the high energy fiber laser and computer-controlled laser beam [3,4]. The schematic diagram of SLM technology is shown in Fig. 1. Further details about SLM procedure and description of parameters are reported in previous study [5]. Due to use of the fiber laser which possesses smaller point size (<100 μm) and more concentrated energy, SLM technique has the highest accuracy than other MAM [6]. Furthermore, it can produce complex geometrical parts with desirable individual shape and internal structure which are both important to bone implant. Thus the SLM-made metallic implants are widely used for orthopedic and dental implants [7,8]. Now, the common medical metal materials containing the titanium and its alloys, Co–Cr alloy, stainless steel and others have been applied in SLM-made implants [9]. Among various metallic biomaterials, titanium and its alloys are the most interesting metallic biomaterials for orthopedic and dental implants due to their excellent mechanical properties, biocompatibility, and good corrosion resistance [10].

However, the major problem concerning with titanium and its alloys in artificial prosthesis is the mismatch of Young's modulus between natural bone (10–30 GPa) and bulk metallic materials (110 GPa for Ti) [11]. This can lead to stress-shielding effect over time, and eventually result in bone resorption and premature failure [12]. A suggestion to overcome this drawback could be the use of porous structure. Furthermore, the porous structure also can form osseointegration and improve fixation by creating a mechanical interlock into the porous structure via the growth of bone [13,14]. The SLM-made porous Ti6Al4V implants had proved to be biocompatible and suitable in vitro cell proliferation [15].

* Corresponding author. Tel.: +86 13296512995; fax: +86 027 87558155.
E-mail addresses: zhangyufeng198785@163.com (S. Zhang), wqs_xn@163.com (Q. Wei), cly0129@126.com (L. Cheng), lisuo@hust.edu.cn (S. Li), shiyusheng@hust.edu.cn (Y. Shi).

http://dx.doi.org/10.1016/j.matdes.2014.05.021
0261-3069/

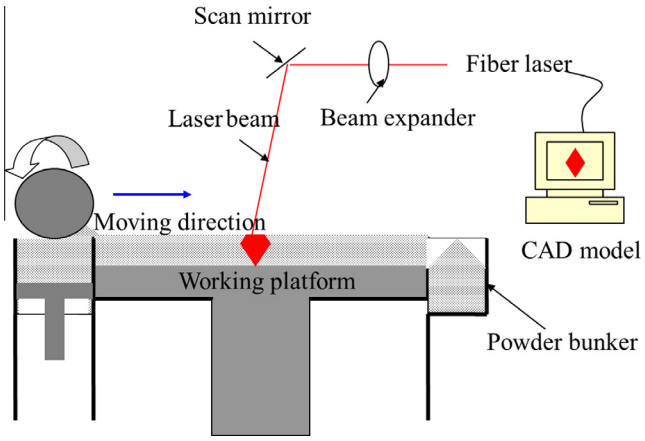

Fig. 1. Schematic diagram of selective laser melting (SLM) process.

In order to fabricate porous implants with high controllability and repeatability by SLM, some methods have been used in previous study. One of the most common methods is using the porous 3D model which is designed by professional software to produce porous structures. For instance, the analog porous bone models, mesh scaffolds and other porous structures with repeating units have been studied in previous researches [16–18]. Some researchers try to add blowing agent into metal powders to form a series of special pores such as honeycomb-like pores [19,20]. However, the complex porous structure made the implant difficult to be designed and fabricated [21]. In comparison, adjusting the process parameters is a convenient way to obtain porous structure in SLM process. This method not only save the time and cost of manufacture but also can be adapted to various complex structures. Only a few researches studied the influence of manufacturing process parameters on the porous structures. Such as, Stamp et al. studied the effects of scanning strategy on porous structures [22] and Gu et al. studied the influence of the processing condition on porous structures [23]. A review of existing literatures reveals that no previous works have been reported about the effect of scan line spacing on the pores morphologies and mechanical characteristic.

Owing to these potential advantages and the relative lack of research on the effects of scan line spacing to porous implant, this investigation aims to gain insight into the influence of scan line spacing on the SLM-made porous implants for biomedical applications. In the work, SLM of Ti6Al4V alloy powder was performed for the preparation of porous structure. The mechanical property, namely porosity, pore connectivity, average pore size, yield strength, Young's modulus and compressive deformation were assessed at different scan line spacing. To satisfy the requirements of pore size of human compact bone, the pore size of the implant was controlled to be smaller than 500 μm by adjusting the spacing of scan line. It provides guidelines for the future design of the compact bone implants with desirable and controllable mechanical properties.

2. Materials and methods

2.1. Materials

Commercial Ti6Al4Valloy powders with fine spherical morphology (shown in Fig. 2a) were used in this study. The powders have an average particle size 65 μm approximately and its particle size distribution is between 20 μm and 120 μm (shown in Fig. 2b). The chemical composition of the powder is listed in Table 1.

2.2. Machine and processing parameters

The forming equipment applied to produce porous Ti6Al4V implants is RPM-II machine, which is developed by Rapid Manufacturing Center of Huazhong University of Science and Technology. A fiber laser (YLP-HP, IPG Photonics Corporation, Germany) with a maximum power of 200 W in continuous laser mode and a spot size of approximately 150 μm is used for the equipment. The forming platform with a vacuum chamber is prepared to prevent oxidation in SLM process. Commercially pure titanium plate with 10 mm thickness was used as the forming substrate plate. The process parameters were optimized in earlier study as follows: a laser power P of 130 W, a scanning speed v of 300 mm/s, a 35 μm layer thickness t. Cylindrical test samples with diameter of 8 mm and length of 10 mm were produced for compression test and porosity characteristic test respectively. After the porous samples were manufactured completely, they were cut by electrical discharge machining (EDM), which ensured plane and parallel end faces of the samples.

2.3. Scanning strategies

In the study, the variable scanning strategies for production of porous Ti6Al4V implants by SLM was described in Fig. 3. Several

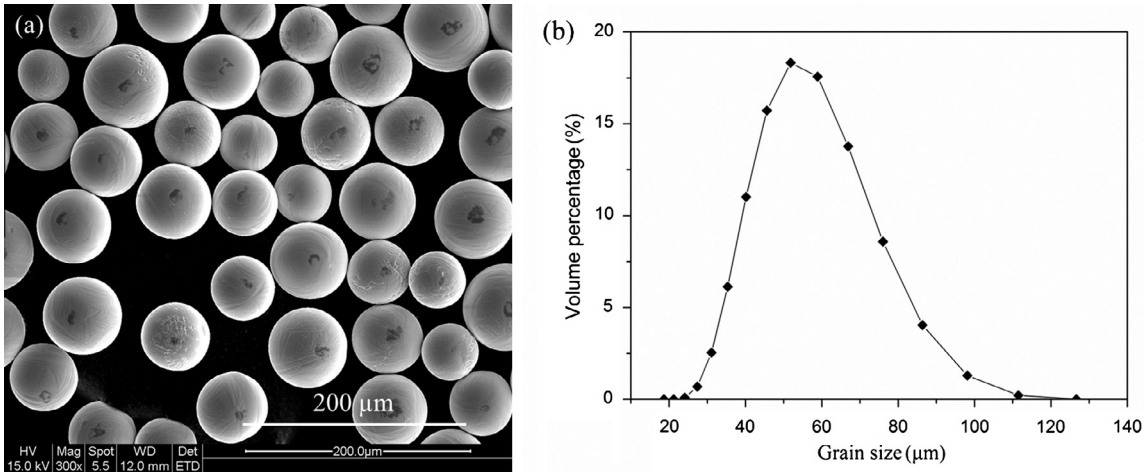

Fig. 2. Characteristics of Ti6Al4V powders: (a) morphology of SEM image and (b) particle size distribution.

Table 1
Chemical composition of Ti6AL4V alloy (wt.%).

Element	Al	V	Fe	C	O	N	H	Ti
Powder (wt.%)	6.0	4.0	0.12	0.02	0.09	0.01	0.002	Balance

steps are shown in the manufacturing process. Firstly, a 3D CAD data is prepared (shown in Fig. 3a), then it is sliced into layers of a defined thickness in horizontal direction (shown in Fig. 3b). The scan lines of each subsequent layer are perpendicular to the former. So it is obvious that SLM process is a repetitive procedure that form powder layers and transfer specific geometrical information into the material by melting the powder with a laser beam. In the study, the scan line spacing was adjusted from 200 μm to 700 μm by a step size of 100 μm to produce porous implants (shown in Fig. 3c). The structures were created by adjusting the laser process parameters to produce walls so that there was no overlap between the individual scan lines.

2.4. Analysis equipment and techniques

The morphologies and microstructure of the porous Ti6Al4V samples were analyzed using a scanning electron microscope (SEM, JSM-7600F, JEOL, Japan). The Pore sizes were measured through the analysis of SEM images. The samples were polished by emery discs, diamond paste and colloidal silicate solution to a finish of better than 1 μm. Polished specimens were etched for 30 s in a solution containing 100 ml H_2O, 5 ml H_2O_2 and 2 ml HF for microstructure analysis. X-Ray Diffractometry (Cu Ka radiation on a PANalytical B.V. diffractometer, Holland) was used for the quantitative analysis of the phase constituents.

Porosity was determined gravimetrically using Eq. (1)from mean dimensional measurements using digital calipers (accuracy 0.002 cm). The specimens mass were measured using digital scales (METTLER TOLEDO, AL204) to an accuracy of 0.01 g.

$$P = 1 - \frac{M/V}{\rho_{Ti}} \tag{1}$$

where P is the porosity of the Ti6Al4V samples, M the mass (g) of samples, V the volume (cm^3), ρ_{Ti} is the density of Ti6Al4V = 4.43 g/cm^3. Bulk density including both open and closed pores of the samples was determined by physical dimensions and mass of the samples. The fraction of open and closed pores in the samples was calculated through the bulk density. The porosity was measured using apparent density via Archimedes principle and bulk density.

Compression tests then were carried out using a mechanical testing machine (SHIMADZU, Japan) applying a 100 KN load cell at a strain rate of 10^{-3} s^{-1}. The main focus of mechanical testing was to determine basic material properties to match with American Society for Testing and Materials (ASTM) standards required for Ti6Al4V implants (**ASTM: E9-09**). Young's modulus and 0.2% proof strength were determined by stress–strain plots which were derived from load–displacement data recorded during compression test.

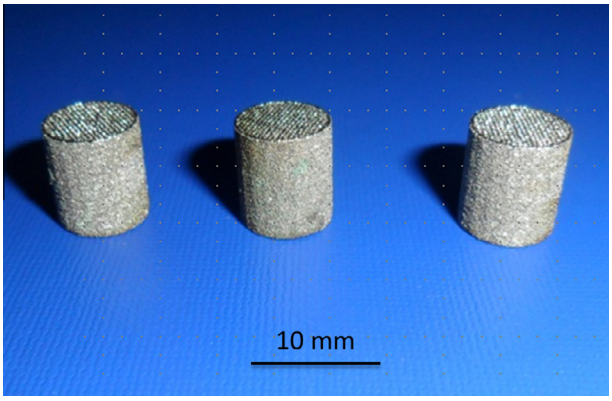

Fig. 4. Typical porous Ti6Al4V implants fabricated via selective laser melting.

3. Results and discussion

The main objective of the experiments described here was to assess the effect of scan line spacing on the porous Ti6Al4V implants. The pores characteristics, mechanical properties and compressive deformation of the porous Ti6Al4V implants formed by changing scan line spacing were analyzed.

3.1. Characteristics of porous Ti6Al4V implants

The photos of typical porous Ti6Al4V implants with different scan line spacing are shown in Fig. 4. The picture shows that the pores can be seen on the top surface and a complete contour can be seen on the side. The micrographs of the pores formed at different scan line spacing were examined by SEM (shown in Fig. 5). The results show that regular and rectangular pores are distributed in the samples and formed by the cross scan line. The thin wall strut sizes of approximately 200 μm were found in all the samples. Through analyzing the scanning strategies (shown in Fig. 3), it is obvious that the thin wall struts were formed by the laser single scan line which depends on spot size of approximately 200 μm. It also indicates that the distance greater than 200 μm is necessary for the pores formed by changing scan line spacing. It is generally accepted that the high porous and interconnected structure is necessary for implants [24]. Fig. 5a shows that a few irregular closed

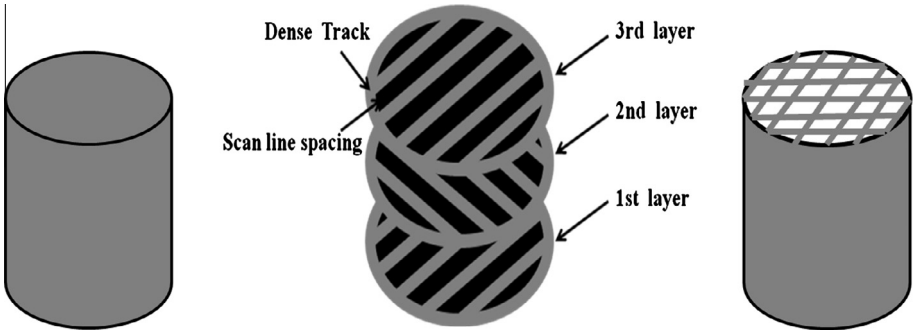

Fig. 3. The schematic diagram of porous implants by changing scan line spacing: (a) 3D solid CAD mode; (b) scanning strategies and (c) stacking of layers to form final dimension.

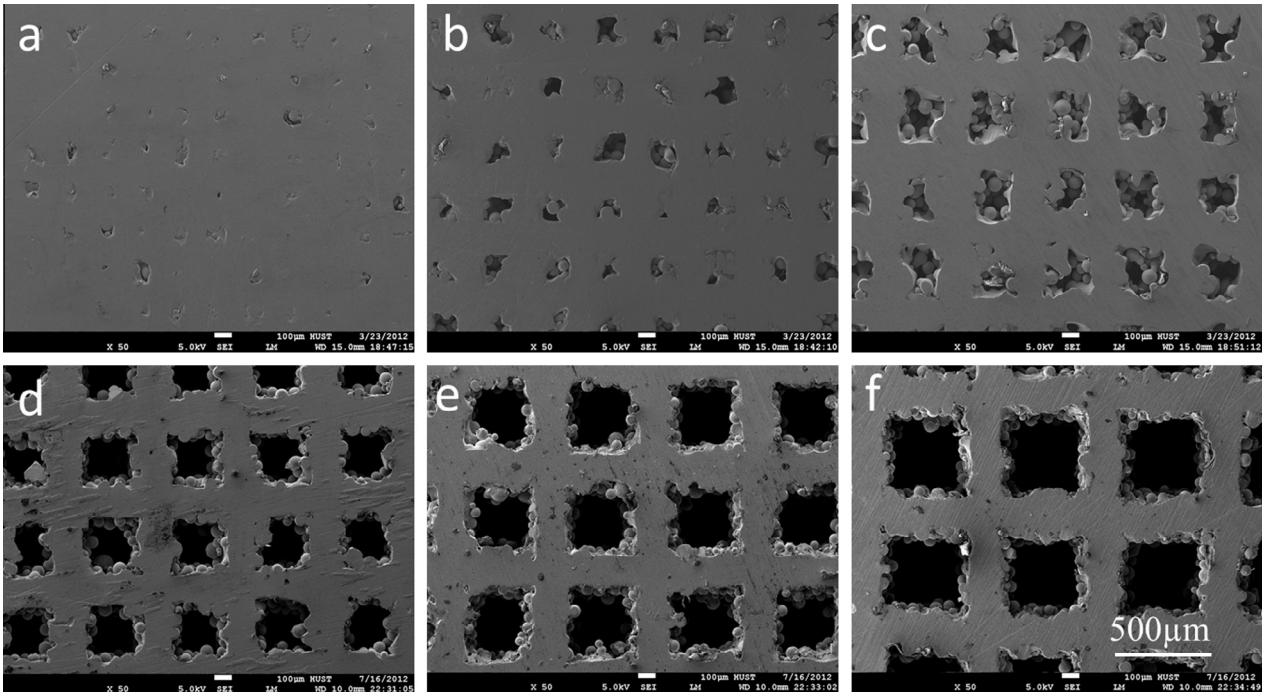

Fig. 5. SEM images of the porous Ti6Al4V implants fabricated by selective laser melting at different scan line spacing: (a) 200 μm; (b) 300 μm; (c) 400 μm; (d) 500 μm; (e) 600 μm and (f) 700 μm.

pores were formed at the scan line spacing of 200 μm. In the study, the powder particle size is in range of 20–120 μm and the mean grain size is approximately 65 μm. It is obviously that it is difficult to form open pores when the pores diameters are smaller than the biggest powders size. With the laser scan line spacing increasing to 300 μm (shown in Fig. 5b), the pores are more obvious but still not open. The pores gradually grow bigger along with the scan line spacing increasing to 400 μm (shown in Fig. 5c), some of the pores are connected but most are closed. In SLM process, a bulk of powder particles is filled in the pores formed by adjacent scan lines. If the pores size is not large enough, the powder particles will not pass the pores and make them disconnected. When the scan line spacing increases to 500 μm (shown in Fig. 5d) or above it (shown in Fig. 5e and f), the channel will have enough space for the powders passing and thus the pores will be interconnected. The result indicates that scan line spacing larger than 500 μm is necessary for the implant with interconnected pores.

For these porous implants, the width of the thin wall is mainly dependent on the laser spot size and the pores which are closed or interconnected are mainly dependent on the powders particle size. In order to form porous structure, especially forming interconnected pores structure, the loose powder particles must be able to pass the channel structure. Generally, when the pore diameter is larger than the biggest size of the powder particles, the powder will pass the channel. However, the partially melted powder particles always adhere on the surface of laser track in SLM process. The schematic of powder particle in the porous structure is illustrated in Fig. 6. As shown in Fig. 6a, a layer of metal particles is scanned by the laser track. As a result, the partially melted particles are bonded to the boundary of each new formed layer. Fig. 6b illustrates a reasonable mechanism for the formation of the open pores in SLM process. When the biggest particles adhere on the laser tracks boundaries and at the same time the biggest powder particles just sandwich between them, the channel will be blocked by the powders. Due to the accumulation effect of the biggest powders, it is necessary that the pore diameter should be three times greater than the biggest powder particles for forming interconnected pore.

Fig. 7 shows the SEM image of the original top surface of the porous implant with scan line spacing of 700 μm. The phenomenon of partially melted raw metal particles on the boundary is clearly visible. The particles have nearly spherical shape with

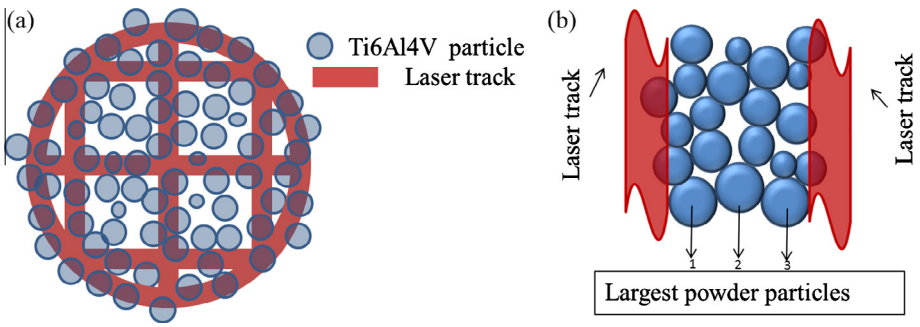

Fig. 6. Schematic of partially melted Ti6Al4V particles in the channel structure: (a) metal particles scanned by the laser track and adhere to their boundaries and (b) the biggest powder particles sandwich between the laser tracks boundaries.

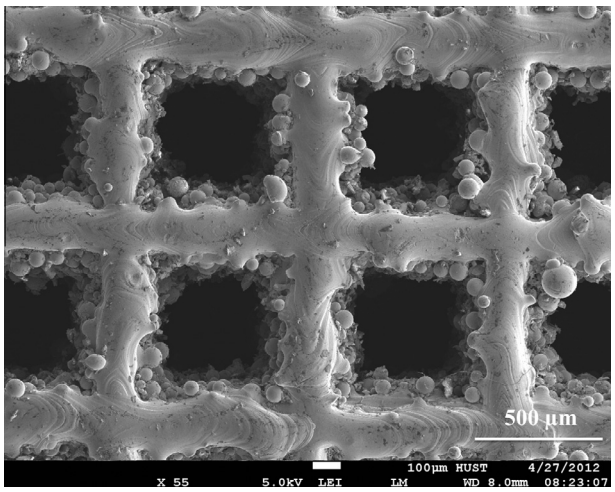

Fig. 7. SEM image of the original top surface of the porous implant with scan line spacing of 700 μm.

particle size of approximately 65 μm. By comparing Figs. 7 and 2a, it can be found that the bonded particle has similar particle size and morphology with the raw Ti6Al4V powder particles prior to melting. This supports the theory further that the bonded particles are caused by partially melted raw powder particles. These bonded particles significantly increase the surface roughness of the samples. Micro-surface roughness has been shown previously to promote osteointegration [25], so it is possible that the rough surface topography of the porous implant will enhance its performance as a bone ingrowth structure.

The relationship of the porosity and size of open pores diameter with the scan line spacing are shown in Fig. 8. It shows that they increased linearly with increasing of scan line spacing. However, from the curve it can be found that the pores which are closed or open have different influence on the porosities at different scan line spacing. The relationship between porosity and scan line spacing in this situation can be described using the following formula:

$$p = C_1 h + C_2 \tag{2}$$

where p is the porosity and h is the scan line spacing. C_1 and C_2 are the constants and can be calculated by fitting the porosity test results. In this study, when the scan line spacing smaller than 500 μm (it means the pores are closed), C_1 and C_2 were calculated to be 6×10^4 and -1.6, respectively. When the scan line spacing

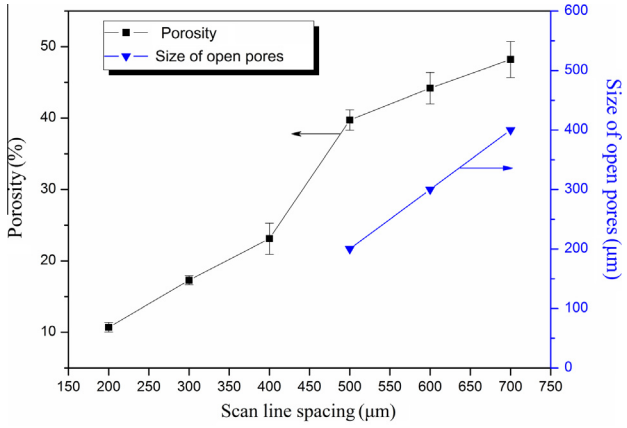

Fig. 8. The influence of scan line spacing on the porosities and sizes of open pores of the porous Ti6Al4V implants.

is above 500 μm (it means the pores are connective), C_1 and C_2 were calculated to be 4×10^4 and 18.6, respectively. In the process of adjusting scan line spacing, the raw powders remain in the porous implant when the diameter of the pore is not large enough and they have effect on the porosity. Thus the scan line spacing has different effect on the porosity for the porous structure within open pore or closed pore. The equation is, therefore, established to use in future designs to estimate the approximate porosity of the SLM-manufactured Ti6Al4V porous structures without experiment testing. What we have shown in the results is that, the scan line spacing be used to tailor porous implants where the porosity can be designed in areas based on the patient's need to enhance biological fixation and achieve long-term in vivo stability.

The pore sizes of the porous implants have been shown to satisfy the requirements for bone ingrowth structures. A potential negative of the variable spacing implants is that the pore distribution is directionally dependent and the pore with rough surface. This may be considered a limitation of this method since there is a special requirement that the bone ingrowth surfaces of orthopedic component closely resemble the bone being replaced. Existing orthopedic metal foams, such as the chemical vapor deposition foam described by Bobyn et al. [26] better achieve this organic appearance.

3.2. Microstructural characterization

As is generally known, microstructure determines mechanical property of the material. Ti6Al4V is a typical two phase α + β titanium alloy. Typical matrix microstructures of as-received Ti6Al4V powder and SLM processed Ti6Al4V samples are shown in Fig. 9. As-received powder and SLM processed Ti6Al4V samples showed a mixture of α and β phases in the microstructures. However, it was found that the SLM processed Ti6Al4V increases the needle-shaped β phase. These observations were confirmed by XRD study on as-received powder and SLM processed Ti6Al4V samples as shown in Fig. 10. The results show that a considerable amount of high-temperature β phases are retained at room temperature in SLM processed Ti6Al4V samples. Sun et al. [27] and Poondla et al. [28] heated the samples to the transformation temperature and cooled them with different rate, and finally observed their microstructures. The microstructures obtained under high cooling rate are same as the microstructure in this study. The martensitic phase is the main microstructure of the SLM processed Ti6Al4V. This is also certificated by Vrancken et al. in their previous studies [29]. Since the fast cooling rate in SLM process (i.e. more than 10^3 K/s), the solid solution atoms V in phase β of Ti6Al4V did not have enough time to diffuse out of unit cells and thus transform into phase α. So the phase β increased in SLM process. However, the martensite transformation is a type of diffusionless transformation [30]. There were no atoms randomly passing or sequentially leaping through the interface and thus the new phase (martensite) shall inherit the chemical composition, atomic order and crystal defects of its parent phase.

3.3. Effect of scan line spacing on compressive properties

The mechanical properties of the porous Ti6Al4V implants were investigated by compression tests. The experimental data shows in Table 2. The experimental data shows that both Young's modulus and yield stress are decreased with increasing scan line spacing. The result shows that the porous Ti6Al4V implants with scan line spacing of 200 μm have mean Young's modulus of 85 GPa and mean 0.2% proof strength of 862 MPa. When the scan line spacing increase to 700 μm, an Young's modulus of 16 GPa and 0.2% proof strength of 467 MPa were produced. However, the scan line spacing has different influence on the yield strengths and the Young's

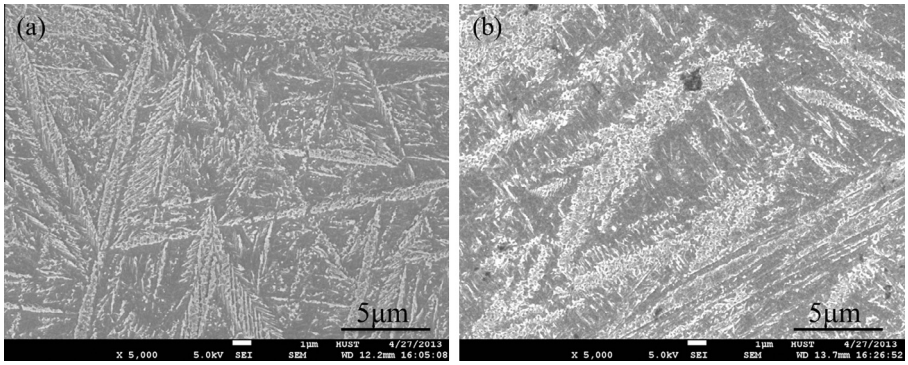

Fig. 9. Typical microstructure of (a) as-received powder and (b) laser processed samples.

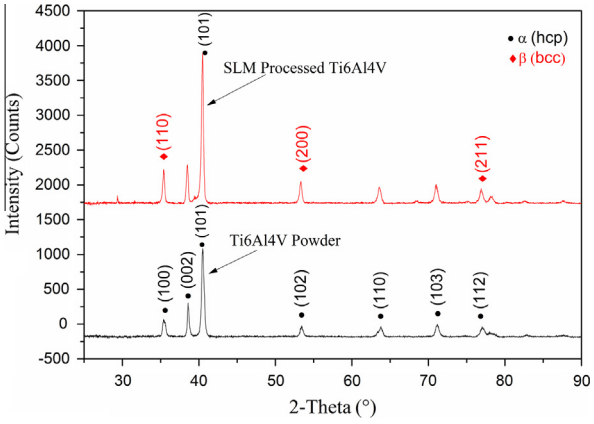

Fig. 10. X-ray diffraction pattern of laser processed structures and as-received Ti6Al4V alloy powder.

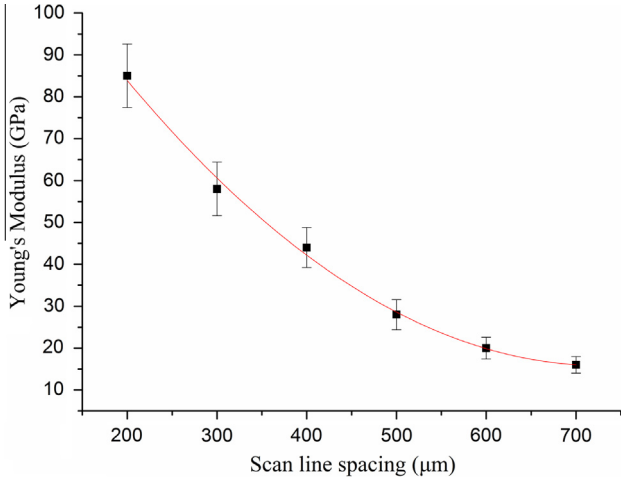

Fig. 11. The variations of Young's modulus of the SLM processed porous Ti6Al4V implants.

Table 2
Yield strength and Young's modulus obtained from the compression tests on the porous samples.

Scan line spacing (μm)	Yield strength (MPa)	Young's modulus (GPa)	Calculated modulus Eq. (2)
200	862 ± 53	85 ± 7.6	63
300	770 ± 50	58 ± 6.4	47
400	686 ± 47	44 ± 4.8	35
500	603 ± 45	28 ± 3.6	16
600	559 ± 42	20 ± 2.6	13
700	467 ± 38	16 ± 2.0	10

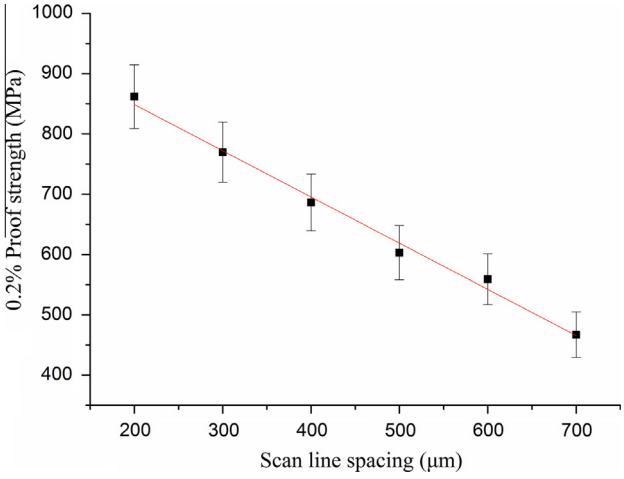

Fig. 12. The variations of 0.2% proof strength of the SLM processed porous Ti6Al4V implants.

modulus. The variations in Young's modulus as a function of scan line spacing are shown in Fig. 11. And the variations of 0.2% proof strength are shown in Fig. 12. The relationship between yield strength and scan line spacing in the study can be described using the following formula:

$$\sigma = C_1 h + C_2 \tag{3}$$

where σ is the 0.2% proof strength and h is the scan line spacing. C_1 and C_2 are the constants and can be calculated by fitting the test results and were calculated to be -766×10^3 and 1×10^3, respectively. And the relationship between Young's modulus and scan line spacing can be described using the following formula:

$$E = C_1 h^2 + C_2 h + C_3 \tag{4}$$

where E is the Young's modulus and h is the scan line spacing. C_1, C_2 and C_3 are the constants and can be calculated by fitting the test results and were calculated to be 2425×10^5, -354×10^3 and 145, respectively. In the study, we can find that the Young's modulus and yield strength of the porous Ti6Al4V implants can be tailored through the above formulas by changing the scan line spacing. Through analysis, we know that the sizes of raw powder particle have an important influence on the formation of the porosity. The laser spot size directly determines the wide of the porous implants' dense wall or structural support. For the same materials,

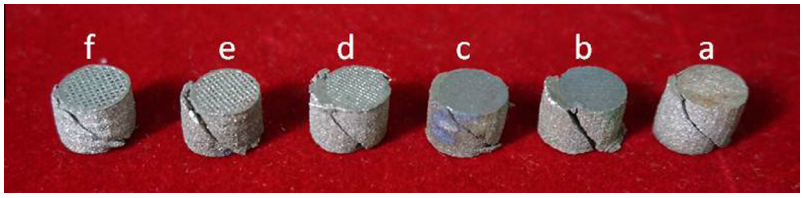

Fig. 13. Deformed samples from compressive test with different scan line spacing (from right to left) (a) 200 μm, (b) 300 μm, (c) 400 μm, (d) 500 μm, (e) 600 μm and (f) 700 μm.

the porosity and sizes of the structural support are the main factors affecting mechanical properties of porous implants. So they can influence the accuracy of the formulas obtained by fitting the experimental data. Chang et al. [31] pointed out the significance of bone in growth under load-bearing conditions. Thus, the load bearing is one of the important functions for implants. Gibson [32] had pointed out that the Young's modulus and compressive strength of compact bone are 3–20 GPa and130–180 MPa in his research. The results indicate that mechanical properties can be designed to satisfy the requirements of human compact bone by changing scan line spacing in SLM process. The porous Ti6Al4V implants with matching properties with compact bone, which can significantly improve bone cell–implant interaction.

For porous elastic materials, the relationship between the elastic modulus and porosity has been widely investigated [33]. An attempt has been made here to estimate the Young's modulus of SLM processed porous Ti6Al4V samples using Nielsen's relationship [34]:

$$E = E_m \frac{(1-v)^2}{1+\left(\frac{1}{\rho}-1\right)v} \tag{5}$$

where E is the Young's modulus of porous material, E_m is the Young's modulus of fully dense material (114 GPa for Ti6Al4V), v is the volume fraction of porosity and ρ is the geometry factor based on pore shape (In the present work, the geometry factor (0.2) was taken as the roundness of the pores computed as: $\frac{4\times\pi\times\text{Area}}{\text{Perimeter}^2}$.). Estimated modulus values using the above equation are compared with experimental values in Table 2. Although slightly higher than experimental values, the modulus calculated using Nielsen's relationship is in good agreement with our experimental values. The discrepancies between the calculated and experimental modulus values are presumably due to the influence of pore geometry and stress concentrations [33]. There is a subtlety that needs to be pointed out in Nielsen's relation which helps explain how one can also tailor the properties of porous metals by changing the shape/geometry factor of the pores.

3.4. Compressive deformation

The pictures of the typical deformed specimens from compressive test with different scan line spacing are shown in Fig. 13(a–f), for scan line spacing from 200 μm to 700 μm, respectively. The 45° orientation of the crack shown in Fig. 13 clarifies the brittle deformation behavior in the porous Ti6Al4V samples i.e., they deformed as a bulk material. The samples which fabricated at different scan line spacing with different pore sizes and different porosities but they have the same thin dense walls in the structure. Therefore, the brittleness of the porous Ti6Al4V implants is

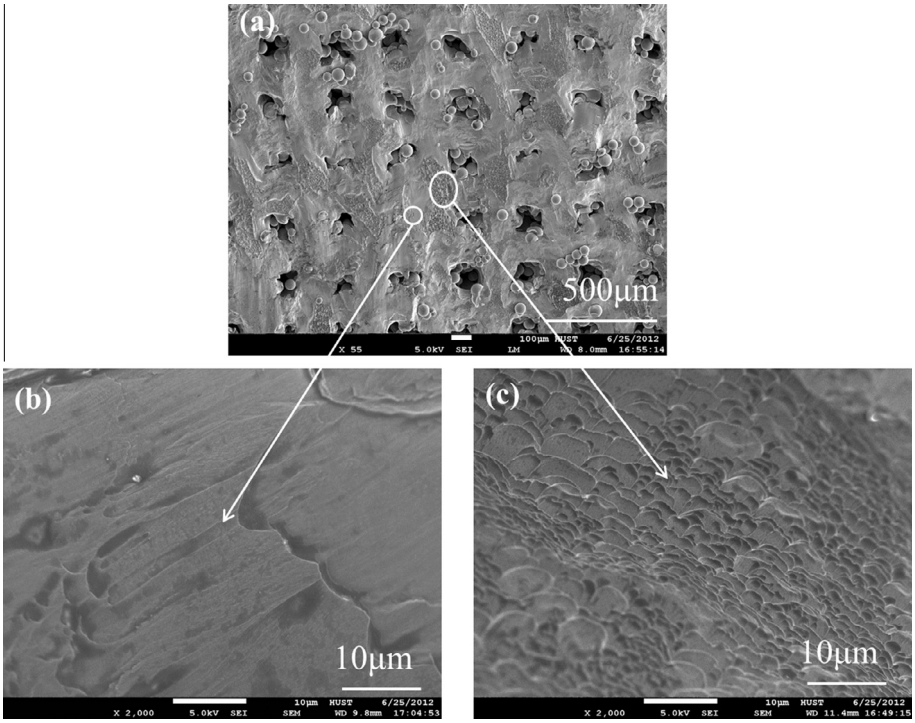

Fig. 14. Micrograph of a typical fracture surfaces (shear plane shown in Fig. 13) for the porous Ti6Al4V sample: (a) scan line spacing of 200 μm, (b) shear slip plane features of the fracture surface and (c) sharp ductile dimple features of the fracture surface.

due to the dense walls rather than the presence of porosity. In addition, it is known that during compressive deformation, dense metals usually fracture in brittle manner with crack orientation of ~45° to the applied stress. Similar brittle deformation behavior was also observed in the porous Ti6Al4V samples during compressive deformation. Therefore, the brittleness of porous Ti6Al4V samples is attributed to the dense walls. Balla et al. in his previous study also find the same phenomenon [35]. Fig. 14 shows the micrograph of a typical fracture surface of one porous sample (Fig. 14a is the fracture surface of scan line spacing of 200 μm). More detailed microstructure analyses was carried out as shown in Fig. 14b and c. As depicted by this figure, the testing samples showed characteristic dimpled structures and the dimples were found to orient along the maximum shear direction (show in Fig. 13). In general Ti6Al4V alloy is a ductile material and SLM processed Ti6Al4V also remained ductile up to failure. Due to the intensive localized deformation, temperature rise, and subsequent cooling shear band showed distinct appearance.

It is well known that titanium alloys are very susceptible to the formation of adiabatic shear band (ASB) [36]. The failure behavior observed above is likely attributed to the ASB formation. The more dominant thermal softening eventually triggers the formation of ASB and leads to catastrophic failure [37]. Furthermore, the pores could likely be a nucleation site for the formation of ASB and subsequent catastrophic failure. For fully dense material, the failure and the corresponding failure strain seem to depend on the duration of the incubation period for developing a nucleation site [37]. Further studies on the failure mechanism behavior of SLM produced porous implants formed by changing scan line spacing, especially the fatigue and fracture toughness, are needed for biomedical applications.

4. Conclusions

This study investigates the effects of scan line spacing on pore characteristics and mechanical properties of porous Ti6Al4V implants fabricated by selective laser melting (SLM). The major findings of this research are:

(1) SEM micrographs analysis show that the porous structure with regular and rectangular pores which can be tailored by adjusting the scan line spacing. The pore diameter should be three times greater than the biggest powder particles for forming interconnected pore whose size ranged in 200–450 μm that can satisfy the needs of compact bone. The convenient method to gain porous implant make it can save time and cost for medical application. But the pore distribution is directionally dependent and this may be considered a limitation of this method.
(2) The fabricated samples with different scan line spacing showed the yield strength in the range of 467–862 MPa and the Young's modulus in the range of 16–85 GPa. They can provide matched mechanical properties with bone tissue. Two equations by fitting the data have been established to use in the future design to estimate the approximate compressive modulus and strength of the SLM-manufactured porous Ti6Al4V structures without mechanical testing.
(3) The main microstructure of the SLM processing Ti6Al4V is martensitic phase which contains a mixture of α and β phases. But, the needle-shaped β phase increases due to the high cooling rate in SLM process. The major failure mechanism of the porous structure is the adiabatic shear band (ASB) fracture and there is no significant influence of the scan line spacing on the failure mechanism.

Acknowledgements

This work has been supported by the founds of State Key Laboratory of Material Processing and Die & Mould Technology in Huazhong University of Science and Technology, China (Grant Nos. 2012-P02 and 2013-09), and National Key Technology R&D Program of Ministry of Science and Technology of China (Grant No. 2012BAF08B03), and National Natural Science Foundation of China (Grant No. 51375189).

References

[1] Melchels FPW, Domingos MAN, Klein TJ, Malda J, Bartolo PJ, Hutmacher DW. Additive manufacturing of tissues and organs. Prog Polym Sci 2012;37:1079–104.
[2] Kruth JP, Froyen L, Van Vaerenbergh J, Mercelis P, Rombouts M, Lauwers B. Selective laser melting of iron-based powder. J Mater Process Technol 2004;149:616–22.
[3] Vandenbroucke B, Kruth JP. Selective laser melting of biocompatible metals for rapid manufacturing of medical parts. Rapid Prototyping J 2007;13:196–203.
[4] Elsen MV, Al-Bender F, Kruth JP. Application of dimensional analysis to selective laser melting. Rapid Prototyping J 2008;14:15–22.
[5] Yasa E, Kruth JP. Microstructural investigation of selective laser melting 316L stainless steel parts exposed to laser re-melting. Proc Eng 2011;19:389–95.
[6] Sun JF, Yang YQ, Wang D. Mechanical properties of Ti–6Al–4V octahedral porous material unit formed by selective laser melting. Adv Mech Eng 2012;2012:1–11.
[7] Jevremovic D, Puskar T, Kosec B, Vukelic D, Budak I, Aleksandrovic S, et al. The analysis of the mechanical properties of F75 Co–Cr alloy for use in selective laser melting (SLM) manufacturing of removable partial dentures (RPD). Metalurgija 2012;51:171–4.
[8] Lindner M, Hoeges S, Meiners W, Wissenbach K, Smeets R, Telle R, et al. Manufacturing of individual biodegradable bone substitute implants using selective laser melting technique. J Biomed Mater Res Part A 2011;97:466–71.
[9] Fox P, Pogson S, Sutcliffe CJ, Jones E. Interface interactions between porous titanium/tantalum coatings, produced by selective laser melting (SLM), on a cobalt–chromium alloy. Surf Coat Technol 2008;202:5001–7.
[10] Song B, Dong SJ, Zhang BC, Liao HL, Coddet C. Effects of processing parameters on microstructure and mechanical property of selective laser melted Ti6Al4V. Mater Des 2012;35:120–5.
[11] Bandyopadhyay A, Espana F, Balla VK, Bose S, Ohgami Y, Davies NM. Influence of porosity on mechanical properties and in vivo response of Ti6Al4V implants. Acta Biomaterialia 2010;6:1640–8.
[12] Bernard S, Balla VK, Bose S, Bandyopadhyay A. Rotating bending fatigue response of laser processed porous NiTi alloy. Mater Sci Eng C – Mater 2011;31:815–20.
[13] Ryan G, Pandit A, Apatsidis DP. Fabrication methods of porous metals for use in orthopaedic applications. Biomaterials 2006;27:2651–70.
[14] Xue W, Krishna BV, Bandyopadhyay A, Bose S. Processing and biocompatibility evaluation of laser processed porous titanium. Acta Biomaterialia 2007;3:1007–18.
[15] Hollander DA, von Walter M, Wirtz T, Sellei R, Schmidt-Rohlfing B, Paar O, et al. Structural, mechanical and in vitro characterization of individually structured Ti–6Al–4V produced by direct laser forming. Biomaterials 2006;27:955–63.
[16] Su XB, Yang YQ, Yu P, Sun JF. Development of porous medical implant scaffolds via laser additive manufacturing. Trans Nonferr Metal Soc 2012;22:181–7.
[17] Warnke PH, Douglas T, Wollny P, Sherry E, Steiner M, Galonska S, et al. Rapid prototyping: porous titanium alloy scaffolds produced by selective laser melting for bone tissue engineering. Tissue Eng Part C Meth 2009;15:115–24.
[18] Yan CZ, Hao L, Hussein A, Raymont D. Evaluations of cellular lattice structures manufactured using selective laser melting. Int J Mach Tools Manuf 2012;62:32–8.
[19] Wang Y, Shen YF, Wang ZY, Yang JL, Liu N, Huang WR. Development of highly porous titanium scaffolds by selective laser melting. Mater Lett 2010;64:674–6.
[20] Shen YF, Gu DD, Wu P. Development of porous 316L stainless steel with controllable microcellular features using selective laser melting. Mater Sci Technol – Lond 2008;24:1501–5.
[21] Wilson JN, Hollister SJ, Riemer BA, Wilson DC. Digital-image-based finite element analysis for bone microstructure using conjugate gradient and Gaussian filter techniques. Math Meth Med Imaging II 1993(2035):95–106.
[22] Stamp R, Fox P, O'Neill W, Jones E, Sutcliffe C. The development of a scanning strategy for the manufacture of porous biomaterials by selective laser melting. J Mater Sci Mater Med 2009;20:1839–48.
[23] Gu DD, Shen YF. Processing conditions and microstructural features of porous 316L stainless steel components by DMLS. Appl Surf Sci 2008;255:1880–7.
[24] Van Bael S, Chai YC, Truscello S, Moesen M, Kerckhofs G, Van Oosterwyck H, et al. The effect of pore geometry on the in vitro biological behavior of human periosteum-derived cells seeded on selective laser-melted Ti6Al4V bone scaffolds. Acta Biomaterialia 2012;8:2824–34.

[25] Anselme K, Bigerelle M. Topography effects of pure titanium substrates on human osteoblast long-term adhesion. Acta Biomaterialia 2005;1:211–22.
[26] Bobyn JD, Stackpool GJ, Hacking SA, Tanzer M, Krygier JJ. Characteristics of bone ingrowth and interface mechanics of a new porous tantalum biomaterial. J Bone Joint Surg Br 1999;81B:907–14.
[27] Sun SD, Zong YY, Shan DB, Guo B. Hot deformation behavior and microstructure evolution of TC4 titanium alloy. Trans Nonferr Metal Soc 2010;20:2181–4.
[28] Poondla N, Srivatsan TS, Patnaik A, Petraroli M. A study of the microstructure and hardness of two titanium alloys: commercially pure and Ti–6Al–4V. J Alloy Compd 2009;486:162–7.
[29] Vrancken B, Thijs L, Kruth JP, Van Humbeeck J. Heat treatment of Ti6Al4V produced by selective laser melting: microstructure and mechanical properties. J Alloy Compd 2012;541:177–85.
[30] Sun J, Yang Y, Wang D. Mechanical properties of a Ti6Al4V porous structure produced by selective laser melting. Mater Des 2013;49:545–52.
[31] Chang YS, Oka M, Kobayashi M, Gu HO, Li ZL, Nakamura T, et al. Significance of interstitial bone ingrowth under load-bearing conditions: a comparison between solid and porous implant materials. Biomaterials 1996;17:1141–8.
[32] Gibson LJ. The mechanical behaviour of cancellous bone. J Biomech 1985;18:317–28.
[33] Krishna BV, Bose S, Bandyopadhyay A. Low stiffness porous Ti structures for load-bearing implants. Acta Biomaterialia 2007;3:997–1006.
[34] Nielsen LF. Elasticity and damping of porous materials and impregnated materials. J Am Ceram Soc 1984;67:93–8.
[35] Balla VK, Bose S, Bandyopadhyay A. Understanding compressive deformation in porous titanium. Philos Mag 2010;90:3081–94.
[36] Liao SC, Duffy J. Adiabatic shear bands in a TI–6A1–4V titanium alloy. J Mech Phys Solids 1998;46:2201–31.
[37] Biswas N, Ding JL, Balla VK, Field DP, Bandyopadhyay A. Deformation and fracture behavior of laser processed dense and porous Ti6Al4V alloy under static and dynamic loading. Mater Sci Eng A 2012;549:213–21.